On the Location-Dependent Quality of the Sensor Pattern Noise and Its Implication in Multimedia Forensics

Chang-Tsun Li[1] and Riccardo Satta[2]

[1]Functional Technologies Ltd, UK
[2]Department of Electrical and Electronic Engineering, University of Cagliari, 09123 Cagliari, Italy
{[1]c-t.li@functional-technologies.co.uk, [2]riccardo.satta@diee.unica.it}

Keywords: Sensor pattern noise, source device identification, multimedia forensics, digital forensics, multimedia authentication, vignetting effect.

Abstract

Due to its uniqueness and potential in forensic applications, the sensor pattern noise (SPN) has drawn much attention in the digital forensic community and academia in the past few years. While much work has been done on the application of the SPN, little investigation into its characteristics has been reported in the literature. It is our intention to fill this gap by providing insight into the dependency of the SPN quality on the location in images. We have observed that the SPN components at the image periphery are distorted to the extent that when used for source camera identification, they tend to cause higher false positive rates. Empirical evidence is presented in this work. We suspect that this location-dependent SPN quality degradation has strong connection with the vignetting effect as they exhibit the same type of location-dependency. We recommend that when image blocks are to be used for forensic investigation, they should be taken from the image centre before SPN extraction is performed in order to reduce false positive rate.

1 Introduction

The combined effect of the fallen prices and increased functionalities of digital imaging devices has allowed them a significant role in many aspects of our everyday life. Powerful and easy-to-use multimedia processing software has also made multimedia manipulation less technical demanding and opened up many new horizons for creative arts. However, it goes without saying that the very same set of tools and technologies also provide means for malicious intention to be realised. As a result, multimedia forensics has emerged as a new and important discipline. Typical multimedia forensic applications include source device identification [1-4], source device linking [5], classification of images taken by unknown cameras [6-8], integrity verification [7, 9], etc.

A typical digital image acquisition process within an ordinary digital camera can be illustrated in a simplified manner as depicted in Figure 1. The light from the scene enters the lens and passes through an anti-aliasing filter before reaching a colour filter array (CFA). According to its predefined colour pattern, the CFA selectively allows one of the red (R), green (G) and blue (B) components of the light per pixel through to the ensuing sensor for conversion into the electronic form. The missing two colours at each pixel are subsequently interpolated by a de-mosaicking process based on the colour configuration within a neighbourhood of the pixel in question. A sequence of image processing operations, such as colour correction, white balancing, Gamma correction, enhancing and JPEG compression, then take place before the photo is stored in the disk. The hardware or software of each stage in the image acquisition pipeline may leave unique "fingerprints" in the content of the image, which can be exploited to identify the imaging devices. As such, to better facilitate forensic investigations, scientists have proposed various ways for extracting those device fingerprints from multimedia content. Sensor pattern noise (SPN) [1, 2, 4, 10], camera response function [11, 12], CFA interpolation artefacts [13, 14], traces of sensor dust [15], JPEG compression [16] and lens aberrations [17, 18] are among the fingerprints that have drawn much attention from scientists.

While many methods [10, 11, 13, 14] can only work when specific assumptions are satisfied, the sensor pattern noise has attracted much interest due to its independence of the similar assumptions. Another desirable aspect of the sensor pattern noise is that it cannot only identify cameras to the accuracy at the model level, but also to the individual camera level [1, 2, 4]. The deterministic component of the sensor pattern noise is mainly caused by manufacturing imperfections and different sensitivity of pixels to light due to the inhomogeneity of silicon wafers [19]. Because of the uniqueness of manufacturing imperfections and the non-uniform sensitivity of each pixel to the light, even sensors made from the same silicon wafer would possess uncorrelated and unique pattern noise. The reader is referred to [19] for more details in relation to the sensor pattern noise.

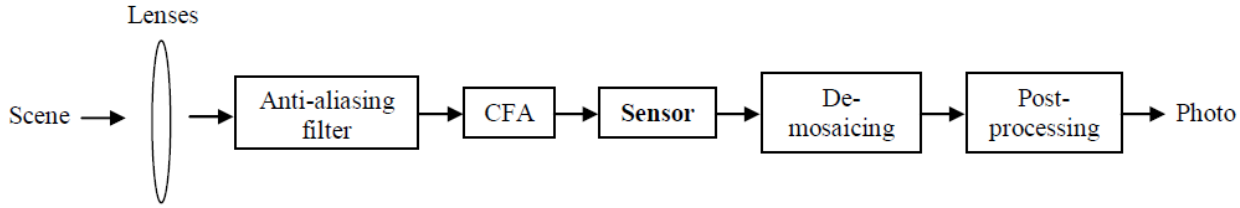

Figure 1. The image acquisition process of an ordinary digital camera.

2 Previous Work

Because, like other types of noise, the sensor pattern noise is present in the high-frequency band in images, most image forensic techniques based on sensor pattern noise [2, 4, 5, 8] adopt the SPN extraction model proposed in [1] or its variant [9]. Let n be the SPN in an image I. The model proposed in [1] can be formulated as

$$n = DWT(I) - F(DWT(I)) \quad (1)$$

where DWT is the Discrete Wavelet Transform and F is a denoising function, which returns the low-frequency components of I. Subtracting the low-passed (denoised) version of I from the original version leaves the high-frequency components of I to be used as the sensor pattern noise. It is easy to see from Eq. (1) that the feasibility of F plays an important role in determining the reliability of the sensor pattern noise. Although different denoising filters can be used as F, the wavelet-based denoising filter presented in the Appendix A of [1] has been known as effective in producing good results. As such, it is used in this work.

SPN matching is necessary in forensic investigations. The normalised cross-correlation defined in Eq. (2) is commonly used to measure the similarity between SPNs n_i and n_j of images i and j:

$$\rho(i, j) = \frac{(n_i - \bar{n}_i) \cdot (n_j - \bar{n}_j)}{\left\| n_i - \bar{n}_i \right\| \cdot \left\| n_j - \bar{n}_j \right\|} \quad (2)$$

where $\bar{n}_i$ and $\bar{n}_j$ are the means of n_i and n_j, respectively. In source device identification, n_j is usually the average of the SPNs from a number of images taken by the same device. If the similarity $\rho(i, j)$ is greater than a threshold, image i is deemed as taken by device j. A commonly adopted threshold is 0.01 [1, 2, 5, 7].

Scene details, such as brick walls, tree leaves and other types of textured surfaces, appear as high-frequency components in images with magnitudes many orders greater than that of sensor pattern noise. Their co-existence with the SPN in the high-frequency band of the images distorts the fidelity of SPN. Aiming at improving the SPNs' performance in digital forensic applications, we have developed an effective SPN enhancer for attenuating the interference of scene details [2]. As the focus of this work is not to demonstrate the performance of the SPN enhancer, but to investigate a common anomaly in the false positive rates when both methods in [1] and [2] are used for source device identification, the reader is referred to [2] for details about the SPN enhancer.

3 Anomaly Reported in Previous Work

Table 3 of [2], which depicts the false positive rates in source device identification, is one of the sets of statistics for validating the proposed SPN enhancer. We have included it as Table 1 in this work to make it self-contained. We use M1 to stand for the SPN extraction model proposed in [1] (i.e., Eq. (1) of this work) and M2 to stand for our proposed SPN enhancer [2]. As reported in [2], we observed an anomaly in Table 1 that, for both methods, when scanning from the right hand side of the table, the false positive rates decrease slightly and reach the minimum when the image block size is 1024 × 1024 pixels. The false positive rates then increase significantly afterwards. This is particularly clearer for the case without enhancement (i.e., M1). After applying other values of the similarity threshold (0.005, 0.015, 0.02, 0.025 and 0.03), we observed the same anomaly. We could not explain the cause of this anomaly at the time of writing [2]. But our recent study into the *vignetting effect* in optics and photography [19-21] has pointed us to look into the possibility that the vignetting effect may have a role in distorting the sensor pattern noise in a *location-dependent* manner. Our experiments, to be presented in Section 4, reveal the fact that blocks taken from locations near the image centre for source identification produce lower false positive rates while blocks from the periphery give rise to significantly higher rates. This has confirmed that the quality of the sensor pattern noise exhibits the similar location-dependent characteristic as that of the vignetting effect. Although due to the lack of our expertise in optics, we are reluctant to definitively conclude that such a location-dependent SPN quality variation is due to the vignetting effect, we would like to

1) present our finding of this location-dependency of SPN quality and
2) recommend that the image borders be avoided if only portions / blocks of the full-size images are needed for forensic applications.

We also hope that this work will encourage further discussions over the possible connection between the vignetting effect and the location-dependent SPN quality degradation in order to gain better understanding of SPN characteristics. Therefore before we present our empirical finding in Sections 4, the vignetting effect is briefly reviewed.

Vignetting is the location-dependent reduction of brightness in optics and photography at the periphery of photos. Brightness is higher in the centre of the images and falls off gradually towards the edges. This also explains the effect that a photographic portrait is usually clearer in the centre and fades off at the periphery. Camera settings and lens design are the main causes of the undesired vignetting effect. Four main types of vignetting due to different reasons are [22]

- Optical vignetting: This type of vignetting is inherent in the lens design and is due to the physical aperture of a multiple element lens. Because the lens has a length, the on-axis light from the scene (corresponding to the image centre) impinges the lens spot-on while the off-axis light (corresponding to image periphery) may be blocked by the lens body. As a result, the effective entrance pupil for the off-axis incident light is reduced, making the image edges appear darker than the image centre.
- Natural vignetting: Also known as natural illumination falloff, natural vignetting is not due to the blocking of light rays, but to the different angles at which the light strikes on different locations of the sensor array. The light has to travel longer from the rear end of the lens (the exit pupil) to the edges than to the centre of the sensor array. The longer the journey is, the greater the loss of light intensity. According to the so-called "cosine fourth" law of illumination falloff, the falloff is proportional to $cos^4\ \theta$, where θ is the angle of the incident light on the sensor array. With a zoom lens, the natural vignetting effect is generally inversely proportional to the focal length.
- Pixel vignetting: Light striking on a photon well in the sensor at a right angle produces a stronger signal than light hitting it at an oblique angle. This angle-dependence of the sensor response also contributes to the falloff of brightness towards the edges of images.
- Mechanical vignetting: This is due to the use of inappropriate attachments to the lens, such as thick or stacked filters, secondary lenses and misaligned lens hoods, that partially block the light path.

Based on the above discussions, we can see that both vignetting effect and false positive device identification rates increase with respect to the distance of the sensor elements / image pixels from the centre. As such, we expect that the vignetting effect is likely to be the cause of the location-dependent SPN quality variation.

Method	False positive rate (%) associated with blocks of various sizes								
	128 ×128	128 × 256	256 × 256	256 × 512	512 × 512	512 ×1024	1024 ×1024	1024 ×2048	1536 ×2048
M1	41.68	38.68	32.60	25.71	16.28	6.75	1.90	2.40	12.03
M2	8.33	3.22	0.95	0.15	0.03	0	0	0.03	0.4

Table 1. False positive rates *with* and *without* applying the SPN enhancer of [2] to the sensor pattern noises extracted with the model proposed in [1]. Note that, in this experiment, the image is deemed as taken by the cameras that are *not* the source camera if their similarity values are greater than a threshold 0.01. The photos contain a wide variety of natural indoor and outdoor scenes taken during holidays, around campus and cities, in offices and laboratories, etc.
M1: Unenhanced sensor pattern noise [1]; **M2:** Enhanced sensor pattern noise [2]

4 Empirical Investigations

As we can see from Table 1, the anomalous changes of false positive rates are more evident when M1 is applied and thus can better facilitate our discussions, we will only use M1 in the following source device identification experiments. To analyse the quality of SPN without the influence of scene details, we use 350 photos of blue sky in JPEG format taken by 7 cameras, each responsible for 50. The JPEG quality factors range approximately from 93% to 97%. The 7 cameras (C_1 to C_7) are Canon IXUS 850IS, Canon PowerShot A400, Canon IXY Digital 500, FujiFilm A602, FujiFilm FinePix A902 and Olympus FE210 and iPhone 4. Apart from iPhone 4, which has a resolution of 1936 × 2592 pixels, the dimensions of the images of the other 6 cameras are 1536 × 2048 pixels. For each camera, the average of 10 SPN blocks, each from one image, taken by the camera is used as its reference SPN block. A SPN block of each individual image is then used to compare its similarity with the reference SPN blocks of the cameras to collect the false positive rates. The normalised cross-correlation defined in Eq. (3) is used to measure the similarity between SPNs n_i of images i and the reference SPN n_c:

$$\rho(i,c) = \frac{(n_i - \bar{n}_i)\cdot(n_c - \bar{n}_c)}{\left\|n_i - \bar{n}_i\right\| \cdot \left\|n_c - \bar{n}_c\right\|}, \quad c \in [1,7] \tag{3}$$

where $\bar{n}_i$ and $\bar{n}_c$ are the means of n_i and n_c, respectively. For each image block, if its smilarity with any camera's reference SPN block is greater then 0.01, this image is deemed as taken by the camera. Therefore, each image may be deemed as taken by more than one cameras.

Table 2 to Table 5 are the *confusion* matrices, which record the *positive rates* (%) when blocks of 512 × 512 pixels taken from various locations of the images are used to identify their source cameras. For example, the value of element (C_2, C_5) is

the positive rate when the SPNs of the 50 image blocks due to Camera C_2 are compared to the reference SPN block of Camera C_5. Because C_2 and C_5 are different cameras, element (C_2, C_5) is actually the *false positive* rate. By the same token, (C_i, C_i), i = 1, 2, …, 7, along the diagonal direction are *true positive* rates.

The image blocks involved in the creation of Table 2 are taken from the *upper-right corner*. To reveal the quality changes of SPN components with respect to their locations in the original images, in the experiment associated with Table 3, we take one block with a 16-pixel displacement in both dimensions from the upper-right corner of the original image. That means 16 pixels at the periphery of each image are discarded and then a block of 512 × 512 pixels is taken from the upper-right corner of the new image. The *true* positive rates along the diagonal direction of Tables 2 and 3 are all 100%, which are not surprising because there are no scene details in the images to distort the SPN. However, the focus of our discussion is the *false* positive rates off the diagonal axis. We can see that they vary quite significantly among cameras because of the quality of the sensors. But it is clear to see that, on average, the false positive rates in Table 3 (9.33%) are significantly lower than those in Table 2 (25.48%). This is clear evidence that the quality of the SPN components closer to the image centre is better than their counterparts closer to the image edges. It is also interesting to see that the blocks associated with Table 3 are only 16 pixels closer to the image centre than the blocks associated with Table 2. As for Table 4, the blocks involved are taken from the location 48 pixels away from the upper-right corner. The average false positive rate is 10.95%, which is slightly higher than that of Table 2 (9.33%). This situation is slightly against our prediction. But conclusion is not to be drawn based on this single instance as the rate difference is small. A clear picture will emerge in Table 5 as well as Table 6 to 8 when blocks taken from a different corner are involved. Table 5 shows the statistics obtained from the same experiment conducted on the blocks taken from the *image centre*. The lower average false positive rate (7.19%) re-conforms to the location-dependency of the SPN quality. The last 3 average false positive rates of the above 4 rates (25.48%, 10.95%, 9.33% and 7.19%) suggest that, generally speaking, the SPN quality of these cameras are relatively stable along the 45˚ direction (towards upper-right corner) until the edge of the image is reached, where the false positive rate increases sharply to 25.48%. But this is not the same situation revealed in the next set of experiment.

Cameras	C_1	C_2	C_3	C_4	C_5	C_6	C_7
C_1	100	8	98	22	96	6	2
C_2	6	100	28	10	20	8	0
C_3	100	10	100	32	100	0	0
C_4	40	22	56	100	64	2	6
C_5	98	20	100	56	100	0	4
C_6	10	14	4	0	0	100	2
C_7	8	2	8	2	6	0	100

Table 2. Confusion matrix. A block of 512 × 512 pixels is taken from the upper-right corner of each full-size image. The rates (%) off the diagonal axis are *false positives* while the rates (%) along the main diagonal direction are actually the *true positives*. When all *false positive* rates associated with all cameras are pooled together the average false positive rate is **25.48%**.

Cameras	C_1	C_2	C_3	C_4	C_5	C_6	C_7
C_1	100	2	2	0	28	10	2
C_2	2	100	16	8	28	14	0
C_3	6	18	100	2	42	2	0
C_4	4	6	10	100	16	6	0
C_5	26	38	58	20	100	0	0
C_6	2	14	0	0	6	100	0
C_7	0	0	0	0	2	2	100

Table 3. Confusion matrix. In this experiment, the 16 pixels along the 4 edges of each image are discarded and then a block of 512 × 512 pixels is taken from the upper-right corner of the new image. The average false positive rate is **9.33%**.

Cameras	C_1	C_2	C_3	C_4	C_5	C_6	C_7
C_1	100	22	2	0	2	50	8
C_2	10	100	20	12	36	10	2
C_3	2	8	100	0	18	2	0
C_4	2	22	10	100	44	4	2
C_5	18	22	22	26	100	16	0
C_6	20	14	8	0	8	100	6
C_7	4	62	0	0	0	0	100

Table 4. Confusion matrix. In this experiment, the 48 pixels along the 4 edges of each image are discarded and then a block of size 512 × 512 pixels are taken from the upper-right corner of the new image. The average false positive rate is **10.95%**.

Cameras	C_1	C_2	C_3	C_4	C_5	C_6	C_7
C_1	100	6	4	0	8	4	0
C_2	6	100	22	10	34	0	0
C_3	10	22	100	2	22	0	4
C_4	0	6	8	100	22	0	0
C_5	6	42	10	4	100	0	16
C_6	12	0	2	0	4	100	4
C_7	0	0	0	0	12	0	100

Table 5. Confusion matrix. In this experiment, one block of 512 × 512 pixels is taken from the centre of the original full-size image. The average false positive rate is **7.19%**.

Table 2 to 4 are associated with blocks taken from (or close to) the upper-right corner of the original image while Tables 6 to 8 contain statistics associated with blocks of the same size (512 × 512 pixels) taken from (or close to) to the *upper-left* corner. We observed that, although the quality degradation of the sensor pattern noise components is proportional to their

distance from the image centre, the SPN quality does not necessarily vary isotropically. The locations of the blocks associated with Tables 6 to 8 are equally distant from the image centre as the blocks associated with Tables 2 to 4. However, we can see that the average false positive rates in Tables 6 to 8 (64.67%, 41.43%, 22.76%) are significantly higher than those in Tables 2 to 4 (25.48%, 10.95%, 9.33%).

We also carried out the same experiments on blocks taken from the lower-left and lower-right corners. When pooling the positives rates across all cameras and four corners of images, the location-dependency of the SNP quality becomes even more evident. The overall average false positive rates are

- 33.70% when blocks are taken directly from the corners (Case 1)
- 19.26% when blocks 16 pixels inward from the corners are used (Case 2)
- 13.56% when blocks 48 pixels inward from the corners are used (Case 3)
- 7.19% when blocks are taken from the image centre (Case 4). Note this rate is lower than that (16.28%) in Table 1 because the images used are all of blue sky with no details while the images used for producing Table 1 are photos containing a wide variety of natural indoor and outdoor scenes taken during holidays, around campus and cities, in offices and laboratories. These natural images contain more details which contaminate the sensor pattern noise and lead to higher false positive rates.

The above experiments have conformed to our expectation that the SPN quality is indeed location-dependent and it is degradated to a greater extent at the image periphery. Figure 2 illustrates the average false positive rate for the above four cases. As such, we can conclude that

- *This explains the anomaly reported in Table 3 of [2]* (duplicated in Table 1 in this work). When full-size images (1536 × 2048 pixels) are used for device identification, although more data is invloved to help with the identification, all SPN components with the poorest quality are also included, which out-weigh the benefit of involving the whole image. By comparing the figures in Table 1, we can see that when only blocks of 1024 × 2048 pixels taken from the image centre are used, the false positive rate drops from 12.03% (when the full-size images are use) to 2.4%. This is because the 256 rows at the top edge and the 256 rows at the bottom edges have been excluded. So even though only 66.67 % (= 1024 / 1536) of the original pixels are used, the exclusion of the SPN components with poorer quality at the periphery allows better performance to be gained. This trend continues as the blocks size is further reduced down to 1024 × 1024. This time not only the 512 rows at the periphery, but also the 1024 columns at the image periphery are excluded. However, when the block size is further reduced down to 512 × 1024, the false positive rates start to increase, indicating that the SPN components of poor quality have been sufficiently excluded and the identifier is starting to suffer from the lack of useful data (i.e., SPN components of better quality).
- In the forensics applications wherein smaller image blocks are required (e.g., blind classification of large image datasets [6-8]), *it is advisable that blocks are taken from the image centre*.
- The higher false positive rates at the image periphery indicate that the SPN similarity / correlation at the image edges is greater. This also suggests that the SPN quality is distorted in the form of *blurring*. This is similar to the fact that the correlation of two smooth signals is greater than the correlation of two high-frequency signals.

Cameras	C_1	C_2	C_3	C_4	C_5	C_6	C_7
C_1	100	66	100	50	100	20	50
C_2	66	100	90	60	98	50	76
C_3	100	100	100	84	100	22	92
C_4	50	70	70	100	86	8	76
C_5	100	100	100	100	100	18	100
C_6	52	56	40	2	54	100	10
C_7	38	62	80	36	74	10	100

Table 6. Confusion matrix. A block of 512 × 512 pixels is taken from the *upper-left* corner of each full-size image. The average false positive rate is **64.67%**.

Cameras	C_1	C_2	C_3	C_4	C_5	C_6	C_7
C_1	100	44	86	20	98	0	18
C_2	34	100	60	42	92	10	54
C_3	74	72	100	28	88	2	32
C_4	38	52	30	100	80	2	32
C_5	100	100	100	92	100	0	84
C_6	8	12	6	16	26	100	8
C_7	10	28	18	8	44	0	100

Table 7. Confusion matrix. In this experiment, the 16 pixels along the 4 edges of each image are discarded and then a block of 512 × 512 pixels is taken from the upper-left corner of the new image. The average false positive rate is **41.43%**.

Cameras	C_1	C_2	C_3	C_4	C_5	C_6	C_7
C_1	100	22	54	2	62	2	0
C_2	48	100	86	8	80	2	0
C_3	48	60	100	22	82	2	0
C_4	8	14	28	100	52	0	0
C_5	30	66	70	28	100	0	22
C_6	8	0	4	4	14	100	0
C_7	4	2	4	2	16	0	100

Table 8. Confusion matrix. In this experiment, the 48 pixels along the 4 edges of each image are discarded and then a block of size 512 × 512 pixels are taken from the upper-left corner of the new image. The average false positive rate is **22.76%**.

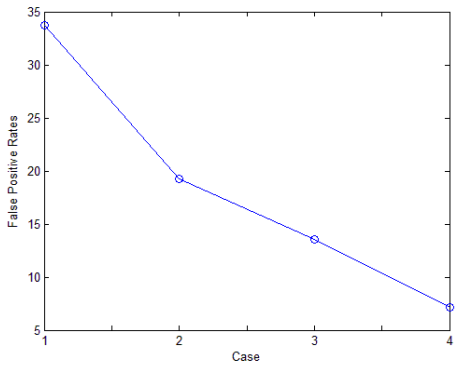

Figure 2. Average false positive rates for four cases. Case 1: blocks taken from the corners; Case 2: blocks 16 pixels inward from the corners; Case 3: blocks 48 pixels inward from the corners; Case 4: blocks taken from the image centre.

5 Conclusion

Sensor pattern noise is of great potential in digital forensic applications. Therefore better understanding of its characteristics and their impact on the accuracy of the information / evidence drawn from forensic analysis is important. We have observed a counter intuitive situation in our previous work that full-size images or image blocks closer to the image periphery tend to give rise to higher false positive rates when used for source camera identification. In this work, starting with the assumption that this anomaly might be related to the vignetting effect due to the lens design and camera settings, we have carried out a series of experiments to see if significant performance discrepancy can be found when the SPN from peripheral blocks and inner blocks are used. The experiments have confirmed that, like the vignetting effect, the SPN quality is indeed location-dependent and explained the cause of the anomaly. Based on the experimental results, our recommendations for the digital forensics communities are:

- Excluding the peripheral pixels of images before the SPN is extracted for source camera identification and linking,
- Taking the blocks from the centre when only small blocks are needed in the applications (e.g., image classification),
- Exercising cautions when dealing with blocks along the image periphery when block-based integrity verification is to be carried out.

References

[1]J. Lukáš, J. Fridrich and M. Goljan, "Digital Camera Identification from Sensor Pattern Noise," *IEEE Transactions on Information Forensics and Security*, vol. 1, no. 2, pp. 205–214, (2006)

[2] C.-T. Li, "Source Camera Identification Using Enhanced Sensor Pattern Noise*," IEEE Transactions on Information Forensics and Security*, vol. 5, no. 2, pp. 280 – 287 (2010)

[3] N. Khanna and E. J. Delp, "Source Scanner Identification for Scanned Documents," in *IEEE International Workshop on Information Forensics and Security*, pp. 166 – 170, UK (2009)

[4]R. Caldelli, I. Amerini, F. Picchioni, A. De Rosa and F. Uccheddu, " Multimedia Forensic Techniques for Acquisition Device Identification and Digital Image Authentication," in *Handbook of Research on Computational Forensics, Digital Crime and Investigation: Methods and Solutions*, C.-T. Li (Ed.), Hershey, PA: Information Science Reference (IGI Global) (2009)

[5]J. Fridrich, "Digital Image Forensic Using Sensor Noise," *IEEE Signal Processing Magazine*, vol. 26, no. 2, pp. 26-37 (2009)

[6]C.-T. Li, "Unsupervised Classification of Digital Images Using Enhanced Sensor Pattern Noise," in *IEEE International Symposium on Circuits and Systems* (ISCAS'10), France (2010)

[7] R. Caldelli, I. Amerini, F. Picchioni and M. Innocenti, "Fast Image Clustering of Unknown Source Images" in *IEEE International Workshop on Information Forensics and Security*, USA (2010)

[8] B.-B. Liu, H.-K. Lee, Y. H and C.-H. Choi, "On Classification of Source Cameras: A Graph Based Approach," in *IEEE International Workshop on Information Forensics and Security*, pp. 1-5, Seattle, USA (2010)

[9] C.-T. Li and Y. Li, "Colour-Decoupled Photo Response Non-Uniformity for Digital Image Forensics," *IEEE Transactions on Circuits and Systems for Video Technology* (accepted, 2011)

[10] H. Gou, A. Swaminathan and M. Wu, "Intrinsic Sensor Noise Features for Forensic Analysis on Scanners and Scanned Images," *IEEE Transactions on Information Forensics and Security*, vol. 4, no. 3, pp. 476 - 491 (2009)

[11] Y.-F. Hsu and S.-F Chang, "Camera Response Functions for Image Forensics: An Automatic Algorithm for Splicing Detection," *IEEE Transactions on Information Forensics and Security*, vol. 5, no. 4, pp. 816 - 825 (2010)

[12] T.-T. Ng and M.-P. Tsui, "Camera response function signature for digital forensics - Part I: Theory and data selection," in *IEEE International Workshop on Information Forensics and Security*, pp. 156 – 160, UK (2009)

[13] A. C. Popescu and H. Farid, "Exposing Digital Forgeries in Color Filter Array Interpolated Images. IEEE Transactions on Signal Processing, vol. 53, no. 10, pp. 3948–3959 (2005)

[14] H. Cao and A. C. Kot, "Accurate Detection of Demosaicing Regularity for Digital Image Forensics," *IEEE Transactions on Information Forensics and Security*, vol. 4, no. 4, pp. 899–910 (2009)

[15] A. E. Dirik, H. T. Sencar and N. Memon, "Digital Single Lens Reflex Camera Identification from Traces of Sensor Dust," *IEEE Transactions on Information Forensics and Security*, vol. 3, no. 3, pp. 539 - 552 (2008)

[16] F. Huang, J. Huang and Y. H. Shi, "Detecting Double JPEG Compression with the Same Quantization Matrix," *IEEE Transactions on Information Forensics and Security*, vol. 5, no. 4, pp. 848 - 856 (2010)

[17] V. T. Lanh, S. Emmanuel and M. S. Kankanhalli, "Identifying Source Cell Phone Using Chromatic Aberration," in *IEEE Conference on Multimedia and Expo*, Beijin, China (2007)

[18] K. S. Choi, E. Y. Lam and K. K. Y. Wong, "Automatic Source Camera Identification Using the Intrinsic Lens Radial Distortion," *Optics Express*, vol. 14, no. 24, pp. 11551-11565 (2006)

[19] J. R. Janesick, *Scientific Charge-Coupled Devices*. SPIE vol. PM83, Bellingham, USA (2001)

[20] H. Hecht, *Optics*. Addison-Wesley (2002)

[21] D. B. Goldman and J.-H. Chen, "Vignette and Exposure Calibration and Compensation," in *IEEE International Conference on Computer Vision*, vol. 1, pp. 899 – 906 (2005)

[22] Ray, S. F.: Applied photographic optics, 3rd ed., Focal Press (2002)